



HAL
open science

Microarray of non-connected gold pads used as high density electric traps for parallelized pairing and fusion of cells

Feriel S Hamdi, Olivier Français, Frederic Subra, Elisabeth Dufour-Gergam,
Bruno Le Pioufle

► To cite this version:

Feriel S Hamdi, Olivier Français, Frederic Subra, Elisabeth Dufour-Gergam, Bruno Le Pioufle. Microarray of non-connected gold pads used as high density electric traps for parallelized pairing and fusion of cells. *Biomicrofluidics*, 2013, 7, pp.044101. 10.1063/1.4813062 . hal-00861239

HAL Id: hal-00861239

<https://hal.science/hal-00861239>

Submitted on 13 May 2015

HAL is a multi-disciplinary open access archive for the deposit and dissemination of scientific research documents, whether they are published or not. The documents may come from teaching and research institutions in France or abroad, or from public or private research centers.

L'archive ouverte pluridisciplinaire **HAL**, est destinée au dépôt et à la diffusion de documents scientifiques de niveau recherche, publiés ou non, émanant des établissements d'enseignement et de recherche français ou étrangers, des laboratoires publics ou privés.

Microarray of non-connected gold pads used as high density electric traps for parallelized pairing and fusion of cells

Feriel S. Hamdi,^{1,2} Olivier Français,¹ Frederic Subra,³
Elisabeth Dufour-Gergam,² and Bruno Le Pioufle^{1,a)}

¹*Ecole Normale Supérieure de Cachan, CNRS, SATIE, UMR 8029, Cachan, France*

²*Univ Paris-Sud, CNRS, Institut d'Electronique Fondamentale, UMR 8622, Orsay, France*

³*Ecole Normale Supérieure de Cachan, CNRS, LBPA, UMR 8113, Cachan, France*

(Received 9 May 2013; accepted 21 June 2013; published online 3 July 2013)

Cell fusion consists of inducing the formation of a hybridoma cell containing the genetic properties of the progenitor cells. Such an operation is usually performed chemically or electrically. The latter method, named electrofusion, is considered as having a strong potential, due to its efficiency and non-toxicity, but deserves further investigations prior to being applicable for key applications like antibody production and cancer immunotherapy. Indeed, to envision such applications, a high amount of hybrid cells is needed. In this context, we present in this paper a device for massive cell pairing and electrofusion, using a microarray of non-connected conductive pads. The electrofusion chamber—or channel—exposes cells to an inhomogeneous electric field, caused by the pads array, enabling the trapping and pairing of cells with dielectrophoresis (DEP) forces prior to electrofusion. Compared to a mechanical trapping, such electric trapping is fully reversible (on/off handling). The DEP force is contactless and thus eases the release of the produced hybridoma. Moreover, the absence of wire connections on the pads permits the high density trapping and electrofusion of cells. In this paper, the electric field mapping, the effect of metallic pads thickness, and the transmembrane potential of cells are studied based on a numerical model to optimize the device. Electric calculations and experiments were conducted to evaluate the trapping force. The structure was finally validated for cell pairing and electrofusion of arrays of cells. We believe that our approach of fully electric trapping with a simple structure is a promising method for massive production of electrofused hybridoma. © 2013 AIP Publishing LLC. [<http://dx.doi.org/10.1063/1.4813062>]

I. INTRODUCTION

Cell fusion is a method to generate a hybrid cell which combines specific properties of its progenitor cells. While cell fusion has been developed for antibody production,¹ it is now also investigated for cancer immunotherapy²⁻⁵ and reprogramming of somatic cells by transferring initialization or differentiation factors.⁶

Different methods inducing the cell fusion are met in the literature, such as the use of viruses,⁷ chemical induction of the fusion using polyethylene glycol,⁸ or physical induction using electric field pulses (electrofusion). The latter method has the advantage to avoid any chemical or genetic contaminations and to achieve higher fusion rate efficiency compared to the chemical method.⁹ Electrofusion becomes thus widely used.^{10,11}

Electrofusion is based on the reversible electroporation of cell membranes induced by electric field pulses.¹² Indeed, during the resealing of contacting permeabilized cells, the

^{a)}Author to whom correspondence should be addressed. Electronic mail: bruno.lepioufle@satie.ens-cachan.fr. Tel.: +33147407736. Fax: +33147402065.

cytoplasmic membranes connect and fuse, leading to the formation of a hybridoma including the cytoplasmic contents of progenitor cells.

The most commonly used system to achieve electrofusion is the electroporation cuvette. Several types of cuvettes are commercialized as BIO-RAD¹³ which is composed of two facing electrodes with 1–4 mm distance, or (Eppendorf¹⁴), composed of ellipsoidal 200 μm distant electrodes. In these cuvettes, a large population of cells (typically more than 10^6 cells) are suspended between the electrodes and the yield of one-to-one cell fusions is very low. Even though the rate of formation of large heterocaryon (more than two cells) is consistent (20% rate),¹⁴ the chance to obtain a hybridoma containing the genetic functions of two different progenitor cells remains very low (of the order of 10^{-4} – 10^{-3} (Ref. 15)).

The use of miniaturized devices to achieve electroporation and electrofusion is investigated since 1990s.^{12,16,17} Such devices permit a better control of the electric field at the scale of the cell, thanks to the electrode patterning, and the possibility to observe the fusion in real time. Nevertheless, a severe bottleneck remains for the development of such biodevices for electrofusion applications, which is the yield of fusion. In particular, when the use of electrofusion is envisioned for immunotherapy, around 2×10^6 hybridoma are needed to make one efficient injection,¹⁸ and a treatment is composed of several injections.¹³

Different strategies for cell trapping and pairing are currently described in the literature such as the grafting of recognition molecules on cells, the use of fluidic forces or dielectrophoresis forces. In the former case, chemical interactions of recognition molecules (as Biotin-Streptavidin¹⁹) grafted on each cell is used for their pairing. This method remains efficient even in the case where cells to be fused present very different sizes and electric properties. Nevertheless, this chemical pre-treatment modifies the membrane structure of cells, and the yield of one-to-one pairing remains low due to the random cell contact.

The use of fluidic forces⁹ is very efficient for high density cell trapping and pairing. However, this strategy requires further improvements for the trapping of cells having different sizes.

An alternative method for cell trapping and pairing is the use of dielectrophoretic forces created by insulators inducing electrical field concentration.^{16,20–24} The last two methods are very efficient for cell pairing and electrofusion but are both coupled with mechanical handling (fluidic and mechanic in the case of Ref. 9, electric and mechanic in the case of Refs. 16 and 22). Indeed, cells are trapped, paired, and fused in fluidic traps for the former, while they are fused through a small orifice in an insulating wall for the latter. However, this mechanical contact with obstacles, useful for maintaining the cells during the fusion, is not convenient for the release and collection of the fusants because the hybridoma might stay blocked in these physical traps.

On the other hand, in the absence of such physical traps, the dielectrophoretic forces might provide a fully reversible way to handle, array, or trap cells on a device,^{25–28} which might be convenient in our case to release and collect hybridoma. Indeed, dielectrophoresis is very popular for cell manipulation.²⁹ Since 2000, many microfluidic devices were developed using dielectrophoresis for the concentration and lysis of cells,³⁰ capture, separation, and study of the electric properties of different cell types,^{28,31–34} circulating tumor cells capture,³⁵ separation of live and dead yeast cells,³⁶ and other applications. These devices are generally based on parallel,³⁶ interdigitated,^{25–27} or arrayed electrodes.²⁸ Nevertheless, in the case of electrofusion, none of these structures cope with the problem of polynuclear fusions. Moreover, the density of electrical traps is limited by the electric wiring and the complexity of microfabrication (addition of multiplexing functions for example).

In this work, we present a new microfluidic biodevice dedicated to electrofusion, which overcomes this limitation. The structure involves an array of non-connected micro-sized electroplated gold pads, positioned between two electrodes, which induce a specific electric field topology. This electric field inhomogeneity gives rise to a dielectrophoretic force (DEP) used for cell trapping and pairing. The absence of wiring and connections, as gold structures are not powered, allows envisioning the high density arraying which will be necessary when the high throughput is targeted for the electrofusion. Successful pairing and fusion of cells in the microarray is demonstrated.

In Sec. III A the design of the device is presented, relying on finite element numerical analysis of the forces produced by the electric field and the fluidics. The effect of the thickness of the metallic pads is investigated to optimize the device, in particular the transmembrane potential of paired cells prior to electrofusion. Experiments demonstrating the capabilities of the device in terms of cell trapping, pairing, and electrofusion are described in Secs. III C–III E. Parallelized electrofusion of paired cells with a yield up to 75% is achieved, as will be shown in the paper. Advantages of the design are (i) non mechanical handling (on/off), (ii) easy release of the hybridoma, (iii) no wiring of the pads, which allows a highly parallelized electrofusion, and (iv) a simple structure with an easy fabrication process, only requiring two standard photolithography steps.

II. MATERIALS AND METHODS

Cell electrofusion on a chip is sequenced as follows: (i) the trapping and pairing of cells, (ii) the application of the electrical pulses that lead to electroporation followed by electrofusion of the membranes, and (iii) the maintaining of the contact between paired cells during the hybridoma formation.

On our device the trapping and pairing of cells is achieved, thanks to dielectrophoresis forces, while the electrofusion phenomena occurs when the transmembrane potential is high enough to induce the membrane electroporation at the contact point of paired cells.

In order to evaluate the effect of the presence of a non-connected conductive pads array on the electric field topology and the consecutive DEP force that appears, as well as the transmembrane voltage induced by the applied electric field pulses that induce the electrofusion, a 3 dimensional finite element analysis was carried out (AC/DC module of COMSOL Multiphysics ©).

A. Numerical computation of the dielectrophoresis force within the device

When a polarisable object, like a biological cell, is immersed in a non-uniform electric field, DEP force appears due to the interaction between the external field and the induced dipole.^{37,38} In the case of stationary electric field, the DEP force for a spherical object is

$$\vec{F}_{DEP} = 2\pi R_{cell}^3 \epsilon_m \Re_e[K_{CM}] \vec{\nabla} |E^2|, \quad (1)$$

where K_{CM} is the Clausius-Mossotti (CM) factor, $\Re_e[K_{CM}]$ its real part, R_{cell} the object (cell) radius, and ϵ_m the medium (extracellular medium) permittivity. The K_{CM} factor can be expressed as follows:

$$K_{CM} = \frac{[\epsilon_c^* - \epsilon_m^*]}{[\epsilon_c^* + 2\epsilon_m^*]}, \quad (2)$$

where ϵ_x^* is the complex permittivity ($\epsilon_x^* = \epsilon_x - i(\sigma_x/\omega)$) with ϵ_x and σ_x being, respectively, the permittivity and the conductivity of the medium (m) or the cells (c) and ω is the electric field pulsation. The sign of K_{CM} determines the direction of the force: if K_{CM} is positive, the force is directed towards high electric field regions (positive DEP). The sign of K_{CM} depends on the electric characteristics of the medium and the cells but also on the applied frequency; for a given cell and medium, one or two crossover frequencies can be defined.³⁹ Generally, live cells exhibit negative DEP at low frequency ($f < 100$ kHz) and positive DEP between the two crossover frequencies.

To generate DEP forces, the electric field inhomogeneity can be induced by the shape and position of the electrodes, thanks to a variation of conductivity⁴⁰ such as the introduction of insulators (conductivity $\sigma_{obstacle} \sim 10^{-7}$ S/m) in a low conductive medium ($\sigma_{medium} \sim 10^{-3}$ – 10^{-2} S/m for frequencies in the range of 0–10 MHz).¹⁶ In our approach, the electric field inhomogeneity is obtained by the introduction of conductive pads ($\sigma \sim 10^{+7}$ S/m).

In this paper we study the effect of conductive pads and show that their replication in well dimensioned arrays produces high density electrostatic pairing and electrofusion traps.

In our conditions, the effect of the so called Induced Charge Electro-Osmosis (ICEO)^{41–44} is negligible compared to the DEP force. Indeed, the ICEO force, due to the charges induced at the interface electrode/electrolyte, is predominant at low frequencies and dramatically decreases above 1.5 kHz,⁴⁴ while we use frequencies above 400 kHz in our study.

The electric potential was calculated using the AC/DC Module of COMSOL Multiphysics[®], with the conditions showed in Figure 1(a).

Following our finite element analysis, the dielectrophoresis force was post-calculated in any domain of the meshed structure, from the solution V of the potential responding to $\Delta V = 0$. The Claussius Mossoti factor K_{CM} was approximated to 0.4 and the cell diameter to $20 \mu\text{m}$. In each element of the meshed domain we calculated the gradient ∇E^2 , and the DEP force from its expression (Eq. (1)).

B. Modelling and design of the biodevice

The pairing and fusion structure consists of an array of non-connected gold pads ($20 \times 50 \mu\text{m}$, gap = $45 \mu\text{m}$) placed between two connected electrodes with a distance of $410\text{--}460 \mu\text{m}$ (Figure 1). The chamber is delimited by an insulating photoresist constituting the microchannel.

In order to evaluate the effect of the metallic pads thickness on the amplitude of DEP force and electric field, numerical calculations were made using finite element method (FEM) with COMSOL Multiphysics[®].

The gold was chosen as a material for the pads because of its biocompatibility and high conductivity. The dimensions that are to be optimized (see Sec. III B (results)) are shown in Figure 1(a).

C. Fabrication of the biodevice

All the materials constituting the device are biocompatible. We followed the process described hereafter (and shown in Figure 2) for the microfabrication:

- The chip was fabricated on a quartz wafer pre-coated with a thin layer of Cr (15 nm chromium to insure adhesion of gold) and 150 nm Au as a primer for electroplating (deposited by sputtering). Gold layer thickness is increased up in an electrolytic bath based on potassium Aurocyanure $\text{KAu}[\text{CN}]_2$.⁴⁵ The applied current density is 0.75 mA/cm^2 .
- A photolithography step (using S1805 photoresist, MicroChem) defined the mask for the electrodes etching.
- A wet etching process (with KI/I_2 for gold followed by Cr etchant MicroChemicals for chromium) defined the electrodes (electric field generation) and the non-connected gold structures (cell positioning). The photoresist was then removed successively by acetone, ethanol, and water baths. The gold thickness was checked using profilometer measurements (DekTak).
- Microfluidic channels were made of thick SU8-2025. That epoxy photoresist was spin-coated ($500 \text{ rpm}/100 \text{ rpm s}^{-1}/5 \text{ s}$ then $3000 \text{ rpm}/500 \text{ rpm s}^{-1}/30 \text{ s}$), soft baked (3 min at

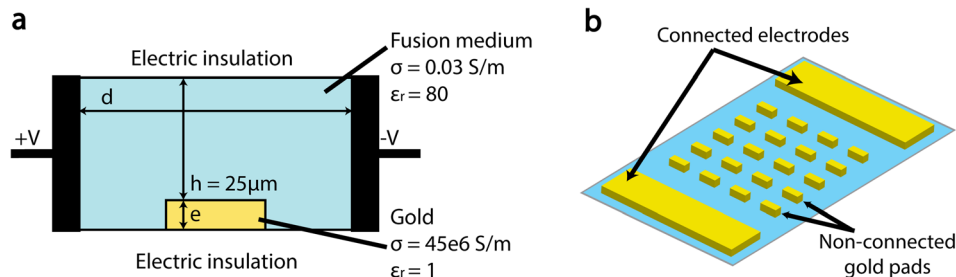


FIG. 1. Simulation conditions: (a) cut view, (b) top view.

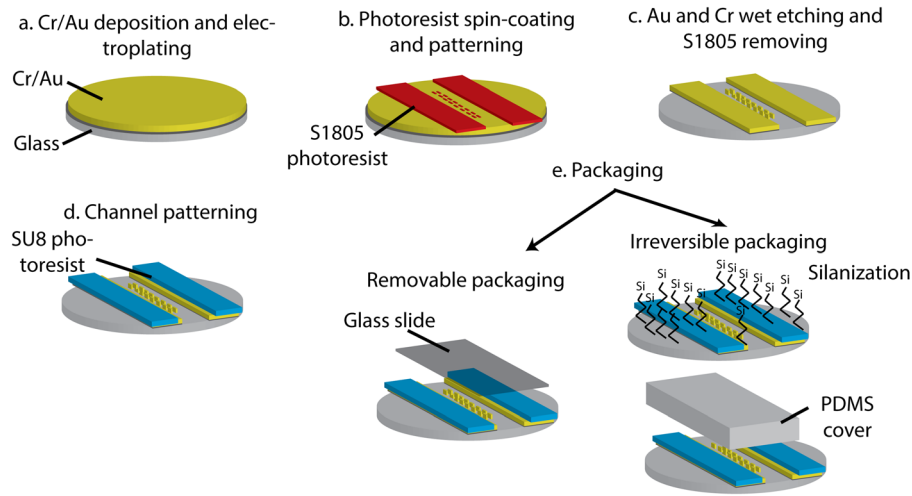


FIG. 2. Microfabrication process.

65 °C, 15 min at 95 °C, and 3 min at 65 °C), insulated (160 mJ), post exposure baked (same 3 steps than the soft bake) and developed to form 25 μm high channels. To get a good adhesion of the photoresist, the device was hard baked during 2 h at 175 °C.

(e) Finally, the device was packaged.

Two different methods for the biochip packaging were used: (i) for the electrofusion tests (presented in Sec. III D), a glass slide was used to cover the chip during the experiment; this reversible packaging was convenient for the cleaning of the biochip. (ii) For the fluidic tests (presented in Sec. III C) an irreversible packaging of a polydimethyl siloxane (PDMS) cover was performed after silanization with (3-aminopropyl)trimethoxysilane (APTMS, Aldrich) of the SU8 and oxygen plasma activation of the PDMS cover.

D. Cell preparation

For biological experiments, mouse melanoma cells B16F10 and human T lymphocyte cells Jurkat had been used. Cells were grown in complete medium defined as minimum essential medium (Invitrogen, Cergy-Pontoise, France) for B16F10 and RPMI (Roswell Park Memorial Institute medium) for Jurkat, supplemented with 10% fetal bovine serum (Invitrogen) and 1% penicillin-streptomycin (Invitrogen). Cultures were maintained in a 5% CO_2 incubator at 37 °C and passed every 2–3 days. Before the experiment, cells were rinsed with PBS (phosphate buffered saline) and detached with Trypsin (Invitrogen) before centrifugation. The cell pellet was then suspended in the hypotonic fusion buffer (0.1 M sorbitol, 0.7 mM MgCl_2 , 0.1 mM calcium acetate, and 1 mg/ml BSA (Bovine Serum Albumin)). The measured conductivity of the medium without cells is 272 $\mu\text{S}/\text{m}$. Low conductivity ensures stronger pDEP and reduces Joule heating. A preparation of 1×10^6 cells/ml was used for the experiments. In the fusion medium, the volume of B16F10 cells is multiplied by 2.4 (new diameter = 20 μm). The same volume change was observed by Sukhorukov² in comparable osmolarity conditions.

E. Experimental setup

When performing fluidic experiments, the flow of cells in the channel was controlled using a microfluidic flow control system (MFCS-4C, FluigentTM).

Two different electric signals were superposed:

- (1) A sinusoidal voltage to generate the DEP force (provided by an AC generator Tektronix AFG 3102),
- (2) Pulses for the electrofusion (provided by Agilent/HP33250A, used in manual burst).

The two electric signals were then added and amplified by a high speed bipolar amplifier (HAS 4101, NF Electronics).

The experimental imaging platform consisted of a reflection microscope (Axio Scope.A1, Carl Zeiss S.A.S) equipped with a high speed camera (Phantom V9.1, Vision Research, AMTEK). The configuration for the video sequence acquisition was 10 pictures/s, 2–40 ms exposition time, and an internal trigger (continuous acquisition).

III. RESULTS AND DISCUSSION

A. Numerical calculation

1. Cell capture

The conducting pad distorts the field topology in which it is immersed (these distortions are shown in Figure 3(a), dark field lines). These inhomogeneities induce a field gradient which leads dipoles—like cells—to experience DEP force. In this section, we study the impact of the thickness of conducting pads on the amplitude of this force.

Figure 3 shows the evolution of DEP forces with the distance from the pad, depending on its thickness.

Near the electrode, the DEP force is almost equivalent for all pads thicknesses. In accordance with the theory, the DEP force is rapidly decreasing with the distance from the pads ($1/d^3$ decreasing law for parallel plate electrodes). However this decrease is even more pronounced for thin electrodes (as shown in Figure 3). As a consequence, the capture zone for the DEP force is larger when thick electrodes are employed. This is a major advantage for the use of thick electrodeposited electrodes.

a. Pairing pattern. Taking advantage of the field concentration effect of one gold pad, we can create a pairing pattern using two pads with a distance equivalent to the size of two cells. Indeed, as shown in Figure 4(a), the pairing zone (between the pads) represents a high electric field area that might capture cells, thanks to positive DEP forces (represented with arrows). If the proper conditions are chosen (appropriate frequency), cells will pair between the pads.

Figure 4(b) shows the evolution of the electric field at $10\ \mu\text{m}$ height for different gold thicknesses. We notice that the E field amplitude is higher for thicker electrodes. Indeed, there is an increase of 16% for $e = 15\ \mu\text{m}$ compared to $e = 150\ \text{nm}$. Furthermore, the pairing zone with thicker electrodes constitutes a physical well for trapped cells.

As summarized in Table I, thick gold pads are advantageous to capture cells from a larger distance and pair them between the pads (the capture zone is larger) and produces a larger electric field between the pads. On the other hand, thick pads require a longer fabrication process (longer electrodeposition and longer chemical etching). The shape factor of the pads has also to

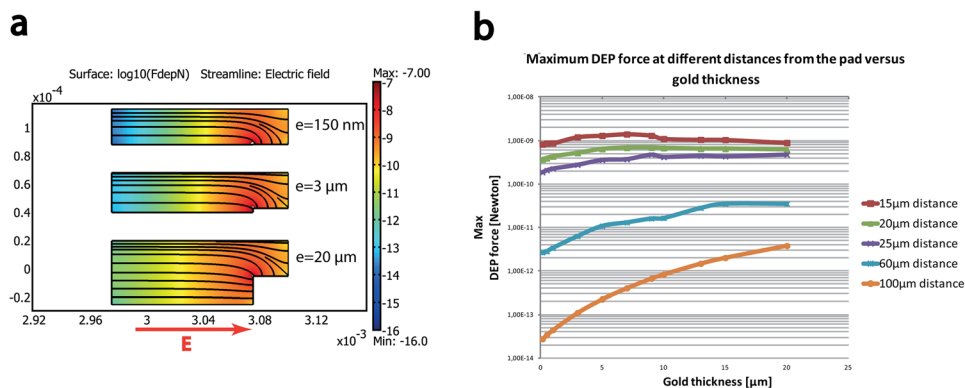


FIG. 3. DEP force versus gold thickness and distance from the electrode: cell's diameter = $20\ \mu\text{m}$ and CM factor = 0.4 (frequencies between 400 kHz and 1 MHz). (a) Colors represent $\log(F_{\text{DEP}})$; (b) evolution of max DEP force at different distances from the pad.

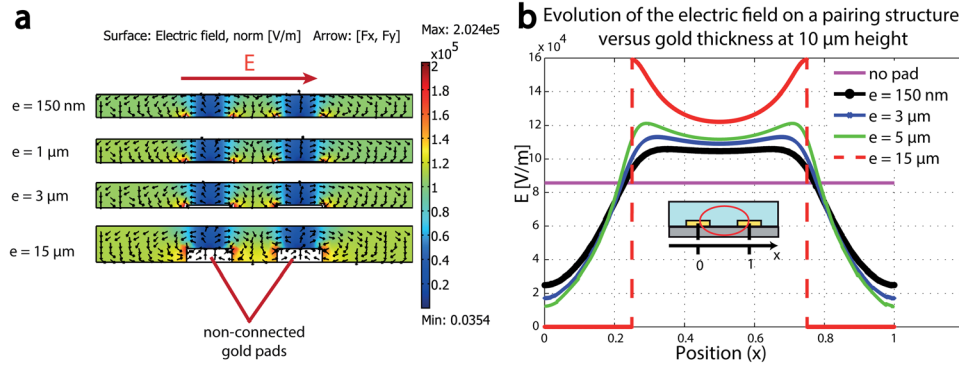


FIG. 4. Simulation of a pairing and fusion structure (two pads) for different gold thicknesses. (a) The electric field and the DEP force (arrows), (b) comparison of the electric field in the pairing zone at $10 \text{ } \mu\text{m}$ height.

be considered when fabricating small surface gold pads. Indeed, the under-etching (due to the isotropic profile obtained with KI/I_2 gold etchant) and the differences in the etching velocities of the electroplated gold and the sputtered primer layer have to be considered. A comparison of the advantages and disadvantages of both thin and thick electrodes is summarized in Table I. Finally a compromise was chosen with $5 \text{ } \mu\text{m}$ thickness gold pads.

b. Arraying. By reproducing the pairing pattern, a microarray structure for the cell pairing and parallelized fusion can be achieved (Figure 5(a)).

Using the 3D AC/DC module of COMSOL Multiphysics, we simulated a structure composed of an array of 6×4 non-connected metallic pads ($10 \text{ } \mu\text{m} \times 40 \text{ } \mu\text{m}$ size separated by $50 \text{ } \mu\text{m}$ distance) between two electrodes ($410 \text{ } \mu\text{m}$ distance). The metal is $5 \text{ } \mu\text{m}$ thick gold, and we applied 50 V on the connected electrodes. The simulation conditions are the same used in Secs. II B–III A.

As shown in Figure 5(a), the gap between pads (parallel to E) constitutes the pairing zone while we apply a sine wave of the adequate frequency to produce positive DEP. Indeed, as shown by the arrows in Figure 5(a), if cells are in low E field areas, they will be brought to the fusion zone (high electric field regions). The gap is dimensioned to the size of two cells in order to avoid multicellular (more than two cells) electrofusions.

In addition, the presence of the non connected gold pads increases the electric field in the pairing and fusion zone (Figure 5(b), with and without pads), which is obvious when we consider that the circulation of the electric field is null within the metallic pads ($E_{\text{interpad}} = V/(d - n \cdot l)$), where E_{interpad} is the field amplitude between the pads, d the distance between the connected electrodes, n the number of pads met by the field line, and l the width of each pad). This homogeneous increase allows reducing the applied voltage during the pairing and fusion steps, which are quite advantageous when one wants to avoid any multiple cells fusion outside of the traps.

c. Electrofusion: Transmembrane potential. Cells being paired and trapped by DEP forces in the microarray, the electric field pulses are then applied in order to induce their electrofusion. These pulses induce a transmembrane potential V_{TMP} , superposed to the natural transmembrane potential (Nernst equation). Once V_{TMP} reaches a critical value, it induces the apparition of

TABLE I. Summary of the effect of gold pad thickness.

Thin gold pads	Thick gold pads
<ul style="list-style-type: none"> • +Easy microfabrication process • –Electric field in the trap is not optimum • –DEP force capture area is reduced 	<ul style="list-style-type: none"> • +Electric field in the trap is increased • +Larger capture area for the DEP force • +Physical trap for paired cells (well) • –Shape factor of the pad is hard to control

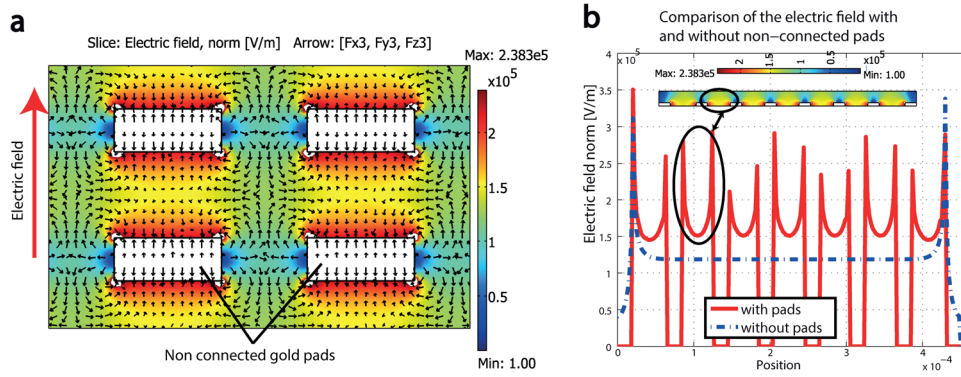


FIG. 5. Pairing and fusion microarray. (a) 3D simulated structure showing electric field topology and DEP direction (arrow, case positive), (b) electric field distribution along a row of pads (continuous curve) and without pads (discontinuous curve).

electropores. However, in the case where V_{TMP} is too high, the membrane electroporation becomes irreversible causing cell death.⁴⁶ Therefore the prediction of the transmembrane potential is crucial to determine the appropriate electric field strength needed for a successful electro-poration prior to electrofusion.

Generally, the electric field is adjusted using the analytical Schwan's law. Thus, considering stationary conditions and a spherical shape for the cell^{47,48}

$$V_{TMP} = \frac{3}{2}ER_{Cell}\cos\theta, \quad (3)$$

with E the amplitude of the applied electric field pulses and θ the angle between \vec{E} and the calculation point on the membrane. Nevertheless, Eq. (3) is only valid in the case of a spherical cell, isolated within a uniform external electric field. As the presence of the other cell changes the shape and the intensity of the electric field, Schwan's law is not applicable in the case of paired cells prior to electrofusion. Thus we used the numerical model described in a previous work²⁴ and compared the transmembrane potential of two contacting cells, with or without the presence of the metallic pads array. This method takes into account the non-homogeneity of the electric field due to the structure and the presence of the other cell. The comparison of the normalized transmembrane potential (V_{TMP}/V_{max} where $V_{max} = 1.5E R_{Cell}$) for an isolated cell (Schwan law), paired cells outside the trap and paired cells in the fusion trap is represented in Figure 6, versus the angular coordinate θ .

As shown in Figure 6, for a given applied external field, V_{TMP} is higher if the cells are positioned within the electrical trap, between the conductive pads. Consequently the electrofusion events will mainly occur for the cells that are trapped, other cells being less excited by the external field (comparison between circle-tagged and triangle-tagged curves). In addition, this polar representation of the transmembrane voltage highlights the fact that the paired cells will be first permeabilized at the opposite poles (higher transmembrane voltage at the opposite pole than at the contacting poles). Consequently by the ionic conduction at the opposite pole membrane, the voltage potential propagates to the contacting pole, leading to an increase in V_{TMP} and membrane permeabilization at the contact of cells to be fused.

B. Fabrication

The device microfabricated following the protocol described in Sec. IIC is shown in Figure 7, placed on the PCB (Printed Circuit Board) dedicated to electric and fluidic connections. A SEM (Secondary Electron Microscopy) view of the structured microarray of conducting pads is shown in Figure 7(b).

As discussed previously, the thick conducting pads are advantageous for cell trapping and fusion efficiencies. Nevertheless, we have to take into consideration the technical limitations linked to the fabrication process. Indeed, the chemical etching with KI/I_2 of gold pads is

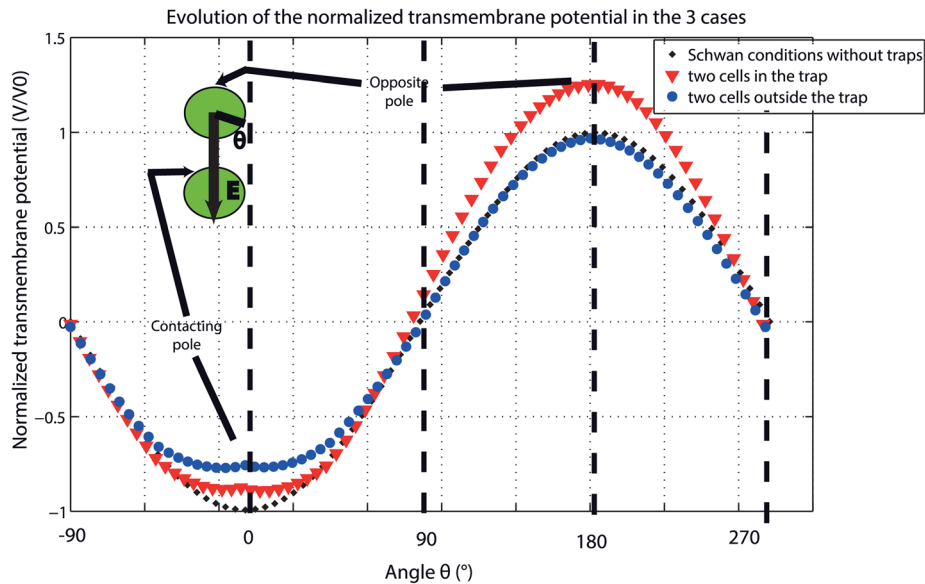


FIG. 6. Normalized transmembrane potential of paired cells inside and outside the trap compared to Schwan law.

isotropic, which leads to an under-etching of the pad in the horizontal direction (this phenomena can be seen in the SEM view in Figure 7(b)). On the other hand, the etching velocity is higher for the primer gold layer (deposited by sputtering) compared to the electroplated layer. Therefore, when the etching ions reach the primer layer, there is a quick under-etching. For a high aspect ratio, an important under-etching causes the removal of the pads. $5\ \mu\text{m}$ thick electrodes were thus chosen as a compromise, as, at this thickness, the under-etching phenomenon is acceptable, while the performances of the device remain interesting (according to numerical simulations in Figure 4).

C. Cell alignment and pairing experiments

For cell alignment, we apply a sinusoidal signal ($U = 20\ \text{V}_{\text{pp}}$, $f = 500\ \text{kHz}$ for positive DEP). Figure 8 shows the typical result of cell alignment and pairing between the gold pads. In the case of low cell concentration, cell pairs are formed in the fusion zone (Figure 8(a)). Therefore, even

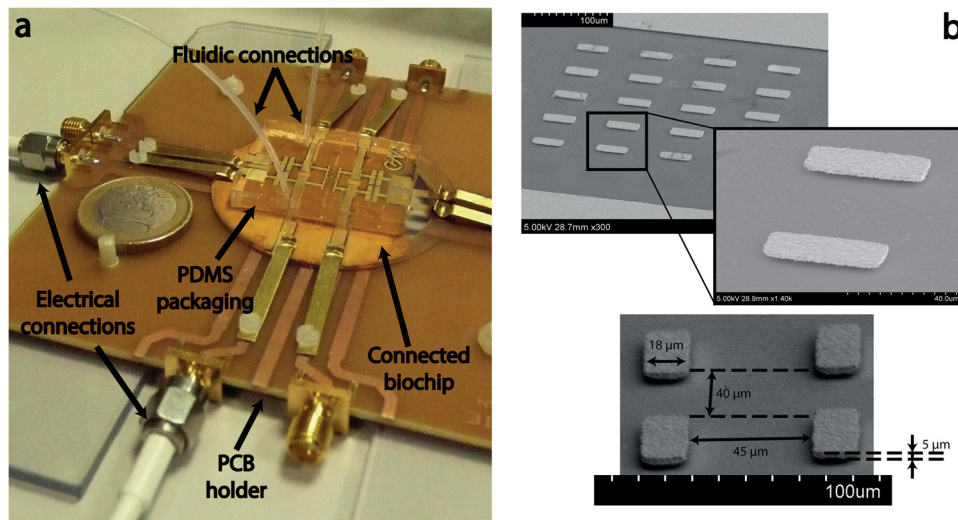


FIG. 7. Microfabrication results: (a) global view of the fabricated chip electrically and fluidically connected on its PCB holder, (b) SEM views and dimensions of the pairing and fusion structure.

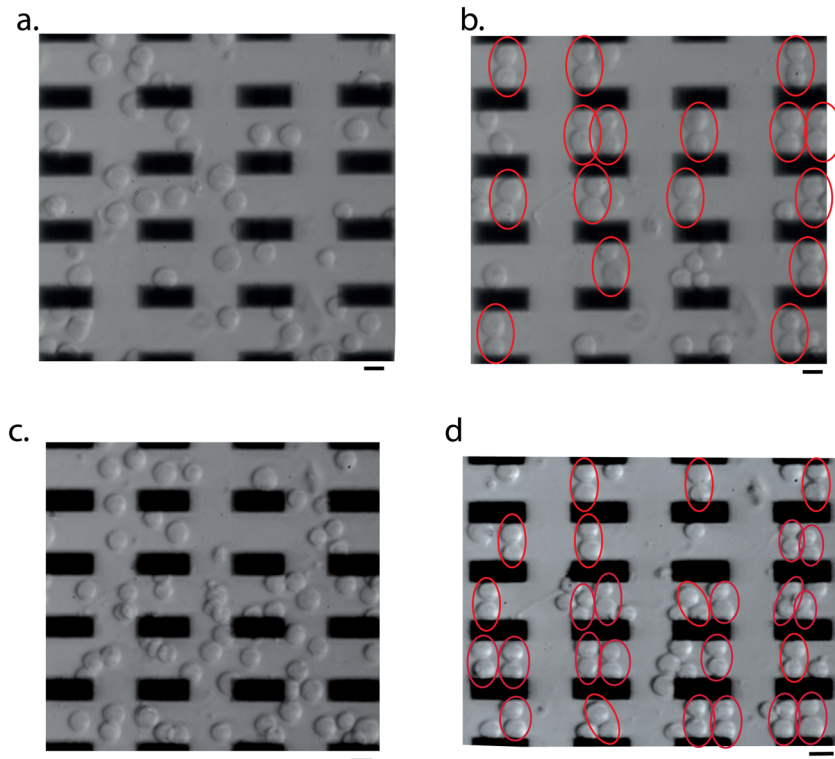


FIG. 8. Trapping and pairing structure, before and after the application of DEP force. (a), (b) Medium density of cells, (c), (d) higher density of cells; even with a high cell density, the cells stay in pairs; scale bars $20\ \mu\text{m}$ (enhanced online). [URL: <http://dx.doi.org/10.1063/1.4813062.1>]

when the concentration of cells is higher, if the trap contains more than 2 cells, they will also assemble as additional pairs disposed between the pads (Figure 8(b)). This property is important for cell electrofusion, as it avoids multicellular hybridomas (more than two cells).

To evaluate the effective DEP force applied on the cell, we use the packaged version of the biochip. Cells are injected in the channel using the MCFS-4C (Fluigent) to control the pressure at the input and the output and thus control the cell velocity. The DEP force is applied simultaneously. Cells are ejected from the pads when the fluidic force prevails. Thus, at the evaluated equilibrium, DEP force equals the fluidic force F_c

$$F_c = \gamma \times v_c, \quad (4)$$

where $\gamma = 6\pi\eta R_{\text{cell}}$ is the friction factor of the cell with the radius R_{cell} in the medium of viscosity η (10^{-3} Pa s). From the experimental determination, DEP force for is about 10 pN (equivalent to a velocity of $50\ \mu\text{m/s}$ for $R_{\text{cell}} = 10\ \mu\text{m}$) while the DEP force calculated by FEM analysis at the center of the trapping zone is 14.5 pN (equivalent to $77\ \mu\text{m/s}$, for $K_{\text{CM}} = 0.4$ and $U = 20\ \text{Vpp}$). We can see that the FEM and experimental results are of the same order of magnitude. Cell trapping and pairing between the pads was successful (as seen in Figure 8).

D. Electrofusion experiments

After the cell pairing was successfully achieved, a train of 10 square pulses (1.3–1.4 kV/cm, $100\ \mu\text{s}$ duration) was applied to induce electrofusion. When we apply 50 V pulses on the connected electrodes, we estimate V_{TMP} at the fusion pole to 1.24 V for paired cells inside the trap and 1 V outside the trap. Fusion thus only occurs within the trap.

Figure 9 shows the dynamics of cell electrofusion in the trapping zone. We could observe that with two (Figure 9(a)) or more (5 cells in Figure 9(b)) trapped cells, only binuclear fusions occur. The design (space between pads or the fusion zone) was calculated to maximize

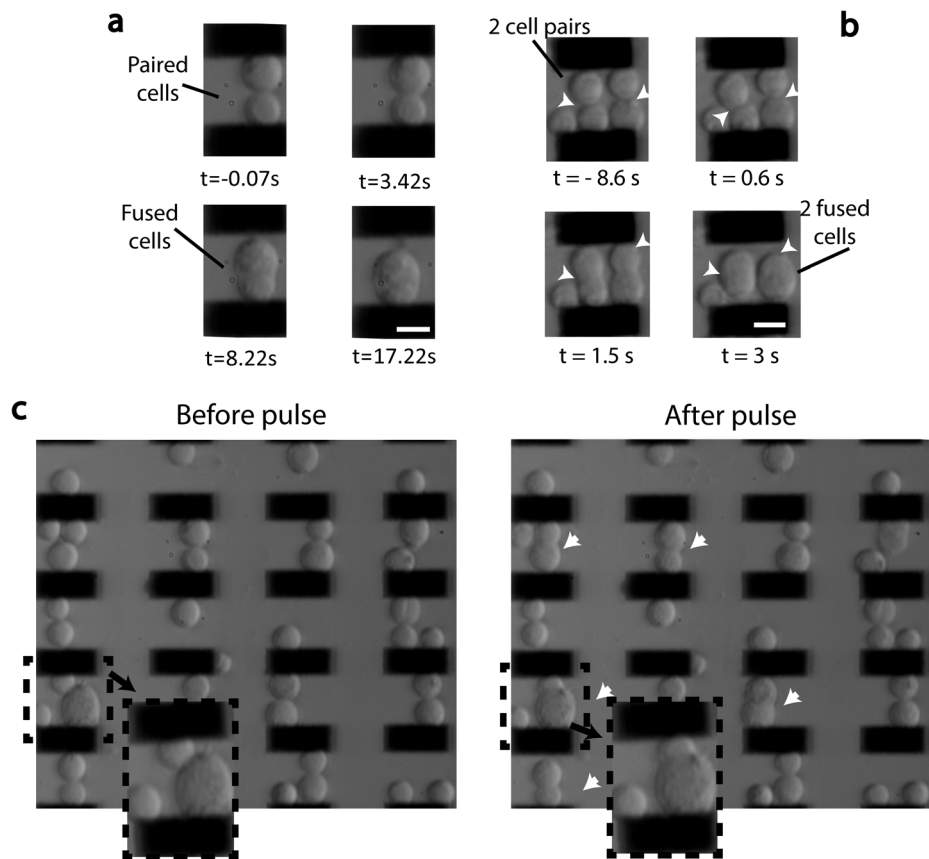


FIG. 9. Dynamics of cell fusion in one pairing structure induced by electric pulses, (a) one pair, (b) two simultaneous fusions on the same pad, no multicellular product, (c) parallel fusions (indicated by white arrows), and a zoom on the fusion of two different cell sizes. Scale bar $20\ \mu\text{m}$ (enhanced online). [URL: <http://dx.doi.org/10.1063/1.4813062.2>] [URL: <http://dx.doi.org/10.1063/1.4813062.3>]

binuclear fusions. Moreover, cells align in the electric field direction. On the other hand, the transmembrane potential is higher at the contact point ($\theta = 0^\circ$) than in the perpendicular direction ($\theta = 90^\circ$, where cells touch unfused cells). As a consequence, only paired cells in the direction of the electric field and in the trap can fuse.

Indeed, we observed that 97% of the fused cells were binuclear (based on 91 fusion events).

The experiment was repeated more than 20 independent times and up to 75% of paired B16F10 cells in the 6×4 matrix of pads were successfully fused. All fusions were binuclear and hybridomas could be ejected from the trap by turning off the DEP force. Furthermore, cells of very different sizes could also fuse (Figure 9(c)). A repeated application of a few pulses increased fusion yield in some cases. This can be due to the thrill caused by the first pulses rearranging the cell pair and improving the contact. Average electrofusion speed was 9.23 s (Based on 83 fusion events, 85.54% of fusions occurred within less than 12 s). Jurkat cells showed the same electrofusion dynamics than B16F10 cells.

Once the cell electrofusion successfully occurred leading to hybridoma, we stopped AC electrical field in order to permit hybridoma collection (Figure 10) for further characterization.

E. Viability and culture tests

Generally, the cell viability is controlled using cell markers, like trypan blue. Nevertheless, this kind of test is not reliable for real time viability evaluation in the case of electroporated cells because the marker massively enters into the permeabilized cell even if it is viable. Thus, we evaluated in a different way the effect of the pulses on the cell viability:

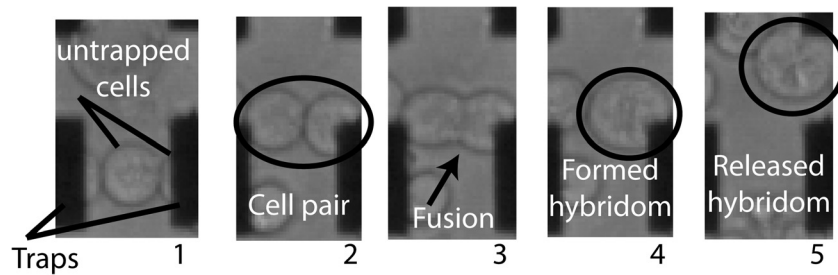


FIG. 10. Capture and fusion of a pair of cells then the release of the formed hybridoma (enhanced online). [URL: <http://dx.doi.org/10.1063/1.4813062.4>]

- (1) We checked visually if the aspect of the pulsed membrane changed. If a difference was noticed, this cell was considered non-viable. If the electric field was too low, no cell fusion was observed. As reported in the literature,¹⁹ cell viability decreases with the electric field amplitude increase, while the electrofusion yield increases. Thus, we gradually increased the electric field amplitude to determine the range where pairs fuse without causing cell lysis. Using this method, we fixed an electric field of 1.1 to 1.25 kV/cm in the trap for the fusion experiments. In that range, we counted 3% dead hybridoma (on 91 fusion events) and 8% lysed cells (on 1043 trapped cells).
- (2) We also checked the viability of produced hybridoma by their culture. After the fusion process, hybridomas were collected and cultured in the complete medium described in Sec. II D. The results are shown in Figure 11. After 3 h, cells adhered confirming their viability. Fused cells showed 2 distinct nucleuses or a bigger one which is probably the result of fused nucleuses. After 24 h, the hybridomas were bigger either with a bigger nucleus (proliferating but not dividing) or polynucleated indicating that the nucleuses divided.
- (3) To confirm hybridoma cell activity, a tetrazolium dye (MTT) was added to the proliferating cells 24 h after the electrofusion process. This dye reduces to purple formazan in the living cells. Formazan crystals formed in the fused cells (Figure 11) confirming their metabolic activity.

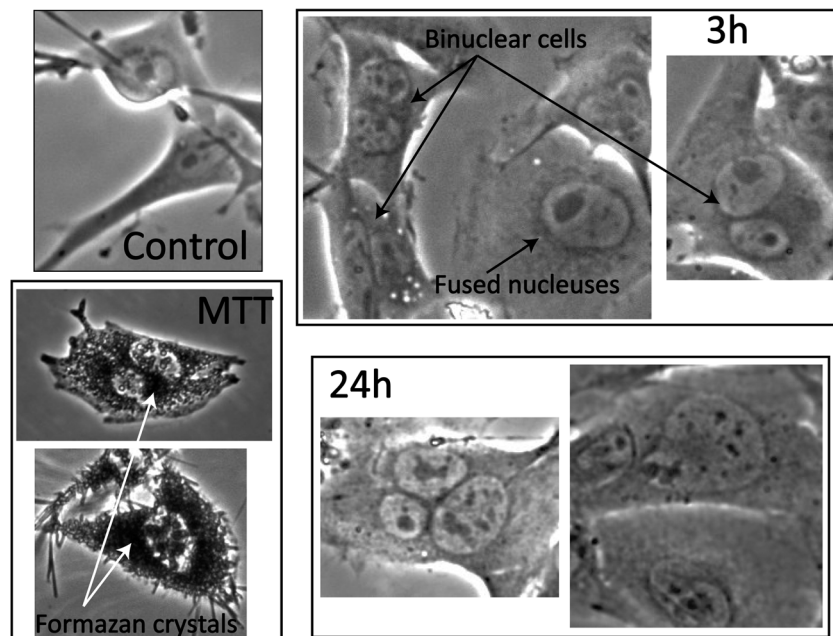


FIG. 11. Culture tests of the fused hybridoma (B16F10) 3 h and 24 h after electrofusion and MTT test on fused and adhered cells. Magnification 40.

IV. CONCLUSIONS

In this study, we described a novel microfluidic device based on the arraying of non-connected electroplated gold pads between two powered electrodes, for high density cell pairing and fusion, and an easy release of the produced hybridomas.

This device has been studied with numerical simulations and was optimised taking into account micro-technological constraints for the thick electrodes fabrication. We showed that the non-connected conductive pads structure generates a field inhomogeneity which initiates the cell pairing by positive dielectrophoresis and their electrofusion, leading to binuclear hybridoma production.

The functionality of the device was validated with two different cell lines. Arraying of cell pairs, followed by successful parallelized electrofusions were observed, while the produced hybridomas were easily released from the reversible electric traps for further culture and characterization. We also demonstrated that the produced hybridomas contain only two nucleuses even in the case of high cell density. Repeated experiments had been achieved to study the efficiency of the microfluidic device. Fast dynamics for the electrofusion process were observed with our conditions, probably due to maintaining the dielectrophoretic force during the application of the fusion electric pulses.

While the tests were carried out with homologous pairs, the presented method remains fully applicable to heterologous cell pairs. Nevertheless, electric properties vary considerably from cell lines to others. The appropriate electric conditions (for positive DEP trapping of both cells and their electrofusion) have to be determined for each type pair.

We believe that the use of microarrays of non-connected conductive pads is a promising technique for high density cell electrofusion on chip, not only for binuclear hybridoma production, but also for the study of the electrofusion process in a parallel way.

ACKNOWLEDGMENTS

This work was performed with the financial support of PRES Universud, CNANO'Ile de France, the ANR PNANO Nanopulsbiochip, and the Labex LASIPS, IMPcell project.

- ¹G. Köhler and C. Milstein, *Nature* **256**, 495 (1975).
- ²V. L. Sukhorukov, R. Reuss, J. M. Endter, S. Fehrmann, A. Katsen-Globa, P. Gessner, A. Steinbach, K. J. Müller, A. Karpas, U. Zimmermann, and H. Zimmermann, *Biochem. Biophys. Res. Commun.* **346**, 829 (2006).
- ³T. Yasuda, T. Kamigaki, K. Kawasaki, T. Nakamura, M. Yamamoto, K. Kanemitsu, S. Takase, D. Kuroda, Y. Kim, T. Ajiki, and Y. Kuroda, *Cancer Immunol. Immunother.* **56**, 1025 (2007).
- ⁴T. Kikuchi, Y. Akasaki, M. Irie, S. Homma, T. Abe, and T. Ohno, *Cancer Immunol. Immunother.* **50**(7), 337 (2001).
- ⁵Y. C. Wei, R. P. Sticca, J. Li, L. M. Holmes, K. E. Burgin, S. Jakubchak, H. Bouton-Verville, J. Williamson, K. Meyer, L. Evans, J. Martin, J. J. Stephenson, S. Trocha, S. Smith, and T. E. Wagner, *Oncol. Rep.* **18**(3), 665 (2007).
- ⁶M. Tada, Y. Takahama, K. Abe, N. Nakatsuji, and T. Tada, *Curr. Biol.* **11**, 1553 (2001).
- ⁷T. Bachi, M. Aguet, and C. Howe, *J. Virol.* **11**(6), 1004 (1973).
- ⁸G. Pontecorvo, *Somatic Cell Mol. Genet.* **1**, 397 (1975).
- ⁹A. M. Skelley, O. Kirak, H. Suh, R. Jaenisch, and J. Voldman, *Nat. Methods* **6**, 147 (2009).
- ¹⁰A. Märten, S. Renoth, T. Heinicke, P. Albers, A. Pauli, U. Mey, R. Caspari, D. Flieger, P. Hanfland, A. Von Ruecker, A. M. Eis-Hübinger, S. Müller, I. Schwaner, U. Lohmann, G. Heylmann, T. Sauerbruch, and I. G. Schmidt-Wolf, *Hum Gene Ther.* **14**(5), 483 (2003).
- ¹¹K. T. Trevor, C. Cathleen, Y. W. Ruiz, E. T. Akporiaye, E. M. Hersh, D. Landais, R. R. Taylor, A. D. King, and R. E. Walters, *Cancer Immunol Immunother* **53**(8), 705 (2004).
- ¹²S. Wang and L. J. Lee, *Biomicrofluidics* **7**, 011301 (2013).
- ¹³U. Trefzer, G. Herberth, K. Wohlan, A. Milling, M. Thiemann, T. Sharav, K. Sparbier, W. Sterry, and P. Walden, *Vaccine* **23**, 2367 (2005).
- ¹⁴D. Zimmermann, U. Terpitz, A. Zhou, R. Reuss, K. Müller, V. L. Sukhorukov, P. Gebner, G. Nagel, U. Zimmermann, and E. Bamberg, *Biochem. Biophys. Res. Commun.* **348**(2), 673 (2006).
- ¹⁵X. Yu, P. A. McGraw, F. S. House, and J. E. Crowe, Jr., *J. Immunol. Methods* **336**, 142–151 (2008).
- ¹⁶S. Masuda, M. Washizu, and T. Nanba, *IEEE Trans. Ind. Appl* **25**, 732 (1989).
- ¹⁷N. Hu, J. Yang, S. W. Joo, A. N. Banerjee, and S. Qian, *Sens. Actuators B* **178**, 63–85 (2013).
- ¹⁸W. M. Siders, K. L. Vergilis, C. Johnson, J. Shields, and J. M. Kaplan, *Mol. Ther.* **7**(4), 498 (2003).
- ¹⁹J. Wang and C. Lu, *Appl. Phys. Lett.* **89**, 234102 (2006).
- ²⁰B. Techaumnat, K. Tsuda, O. Kurosawa, G. Murat, H. Oana, and M. Washizu, *IET Nanobiotechnol.* **2**(4), 93 (2008).
- ²¹M. Kirschbaum, C. R. Guernth-Marschner, S. Cherré, A. Pna, M. S. Jaeger, R. A. Kroccek, T. Schnelle, T. Mueller, and C. Dusch, *Lab Chip* **12**, 443 (2012).
- ²²Y. Kimura, M. Gel, B. Techaumnat, H. Oana, H. Kotera, and M. Washizu, *Electrophoresis* **32**, 2496–2501 (2011).

- ²³G. Mottet, B. Le Pioufle, and L. M. Mir, *Electrophoresis* **33**(16), 2508 (2012).
- ²⁴F. S. Hamdi, O. Français, S. Subra, W. Wang, M. Woytasik, E. Dufour-Gergam, and B. Le Pioufle, *Eur. Phys. J.: Appl. Phys.* **62**(1), 11202 (2013).
- ²⁵G. Tresset and S. Takeuchi, *Biomed. Microdevices* **6**, 213–218 (2004).
- ²⁶J. Ju, J. M. Ko, H. C. Cha, J. Y. Park, C. H. Im, and S. H. Lee, *J. Micromech. Microeng.* **19**, 015004 (2009).
- ²⁷A. I. Clow, P. T. Gaynor, and B. J. Oback, *Biomed. Microdevices* **12**, 777–786 (2010).
- ²⁸M. Frenea, S. P. Faure, B. Le Pioufle, P. Coquet, and H. Fujita, *Mater. Sci. Eng. C* **23**(5), 597 (2003).
- ²⁹R. Pethig, *Biomicrofluidics* **4**, 022811 (2010).
- ³⁰C. Church, J. Zhu, G. Huang, T.-R. Tzeng, and X. Xuan, *Biomicrofluidics* **4**, 044101 (2010).
- ³¹S. Velugotla, S. Pells, H. K. Mjoseng, C. R. E. Duffy, S. Smith, P. De Sousa, and R. Pethig, *Biomicrofluidics* **6**, 044113 (2012).
- ³²A. Salmanzadeh, H. Kittur, M. B. Sano, P. C. Roberts, E. M. Schmelz, and R. V. Davalos, *Biomicrofluidics* **6**, 024104 (2012).
- ³³M. Alshareef, N. Metrakos, E. J. Perez, F. Azer, F. Yang, X. Yang, and G. Wang, *Biomicrofluidics* **7**, 011803 (2013).
- ³⁴S.-H. Liao, C.-Y. Chang, and H.-C. Chang, *Biomicrofluidics* **7**, 024110 (2013).
- ³⁵S. Shim, K. Stemke-Hale, A. M. Tsimberidou, J. Noshari, T. E. Anderson, and P. R. Gascoyne, *Biomicrofluidics* **7**, 011807 (2013).
- ³⁶S. Patel, D. Showers, P. Vedantam, T.-R. Tzeng, S. Qian, and X. Xuan, *Biomicrofluidics* **6**, 034102 (2012).
- ³⁷H. Fricke, *J. Appl. Phys.* **24**, 575 (1924).
- ³⁸H. A. Pohl and I. Hawk, *Science* **152**, 647 (1966).
- ³⁹Z. R. Gagnon, *Electrophoresis* **32**(18), 2466 (2011).
- ⁴⁰K. Khoshmanesh, S. Nahavandi, S. Baratchi, A. Mitchell, and K. Kalantar-Zadeh, *Biosens. Bioelectron.* **26**(5), 1800 (2011).
- ⁴¹T. M. Squires and M. Z. Bazant, *J. Fluid Mech.* **509**, 217–252 (2004).
- ⁴²S. E. Yalcin, A. Sharma, S. Qian, S. W. Joo, and O. Baysal, *Electrophoresis* **31**, 3711–3718 (2010).
- ⁴³S. E. Yalcin, A. Sharma, S. Qian, S. W. Joo, and O. Baysal, *Sens. Actuators B* **153**(1), 277–283 (2011).
- ⁴⁴C. Canpolat, S. Qian, and A. Beskok, *Microfluid. Nanofluid.* **14**(1–2), 153–162 (2013).
- ⁴⁵C. Dalmay, J. Villemejeane, V. Joubert, O. Français, L. M. Mir, and B. Le Pioufle, *Sens. Actuators B* **160**(1), 1573 (2011).
- ⁴⁶E. Tekle, R. D. Astumian, and P. B. Chock, *Proc. Natl. Acad. Sci. U.S.A.* **88**(10), 4230 (1991).
- ⁴⁷H. P. Schwan, *Advances in Biological and Medical Physics*, edited by J. H. Lawrence and C. A. Tobias (Academic Press, New York, 1957), Vol. 5, p. 147.
- ⁴⁸U. Zimmermann and W. M. Arnold, *J. Electrostat.* **21**(2–3), 309 (1988).